



Modelling and simulation of a lava flow affecting a shore platform: a case study of Montaña de Aguarijo eruption, El Hierro (Canary Islands, Spain)

C. Prieto-Torrell, A. Rodriguez-Gonzalez, M. Aulinas, J. L. Fernandez-Turiel, M.C. Cabrera, C. Criado & F. J. Perez-Torrado

To cite this article: C. Prieto-Torrell, A. Rodriguez-Gonzalez, M. Aulinas, J. L. Fernandez-Turiel, M.C. Cabrera, C. Criado & F. J. Perez-Torrado (2021) Modelling and simulation of a lava flow affecting a shore platform: a case study of Montaña de Aguarijo eruption, El Hierro (Canary Islands, Spain), Journal of Maps, 17:2, 516-525, DOI: [10.1080/17445647.2021.1972853](https://doi.org/10.1080/17445647.2021.1972853)

To link to this article: <https://doi.org/10.1080/17445647.2021.1972853>



© 2021 The Author(s). Published by Informa UK Limited, trading as Taylor & Francis Group on behalf of Journal of Maps



[View supplementary material](#)



Published online: 13 Sep 2021.



[Submit your article to this journal](#)



Article views: 643










[View related articles](#)



[View Crossmark data](#)



Modelling and simulation of a lava flow affecting a shore platform: a case study of Montaña de Aguarijo eruption, El Hierro (Canary Islands, Spain)

C. Prieto-Torrell ^a, A. Rodriguez-Gonzalez ^b, M. Aulinas ^a, J. L. Fernandez-Turiel ^c, M.C. Cabrera ^b, C. Criado ^d and F. J. Perez-Torrado ^b

^aDepartament de Mineralogia, Petrologia i Geologia Aplicada, Facultat de Ciències de la Terra, Universitat de Barcelona (UB), Barcelona, Spain; ^bInstituto de Estudios Ambientales y Recursos Naturales (i-UNAT), Universidad de Las Palmas de Gran Canaria (ULPGC), Las Palmas de Gran Canaria, Spain; ^cGeosciences Barcelona, GEO3BCN, CSIC, Barcelona, Spain; ^dDepartment of Geography and History, Facultat de Humanidades, Universidad de La Laguna (ULL), La Laguna, Spain

ABSTRACT

Recent subaerial volcanism at El Hierro Island (Canary Islands, Spain) consists of monogenetic volcanic fields. This volcanism generated cinder cones, tephra air-fall deposits, and lava flows. The lava flows reach several kilometres in length extending through shore platforms and, sometimes, penetrating under the sea level. The volcanic landforms of El Hierro convert it into a natural laboratory for topographic and morphometric modelling and lava flow simulations. We perform the modelling and simulation of the Montaña de Aguarijo eruption, a cinder cone at the NE rift. The associated lava flow channelled through a V-shaped ravine until reaching a cliff, where formed cascades. The flow spread at the cliff base over a platform before reaching the sea modifying the coastline. Different maps were designed to show the results, including the geomorphologic reconstruction of the area affected by this eruption and the lava flow simulations obtained with the Q-LavHA plugin.

ARTICLE HISTORY

Received 5 May 2021
Revised 10 August 2021
Accepted 17 August 2021

KEYWORDS

Lava flow; Digital Elevation Model; simulation; Q-LavHA; El Hierro

1. Introduction

Modelling and simulating volcanic lava flows help evaluate volcanic hazards associated with monogenetic basaltic eruptions and support safe strategies. The resulting maps are critical when applied to volcanic zones where lava flows represent the main hazard for people and properties (e.g. Nieto-Torres et al., 2021; Rodriguez-Gonzalez et al., 2021). While some maps are based on qualitative analysis of historical eruptions, modern assessment combines the geological history with probabilistic or deterministic computational models (e.g. Cappello et al., 2016; Cordonnier et al., 2015; Damiani et al., 2006; de' Michieli Vitturi & Tarquini, 2018; Dieterich et al., 2017; Favalli et al., 2009; Richter et al., 2016; Sieron et al., 2019; Tarquini et al., 2019). The Digital Elevation Model (DEM) of pre-flow topography and the vent location are essential. In addition, physical and rheological parameters of magma are required for simulation using a deterministic approach. In this work, pre- and post-eruptive DEMs are the product of an accurate 3D palaeogeomorphological reconstruction of landforms before and after the studied eruptive event, based on fieldwork. In both cases, the tridimensional reconstruction of palaeosurface follows the methodology of Rodriguez-Gonzalez et al. (2010), aiming to be closer to reality than previous formulae-derived methods.

Fieldwork is the first stage to obtain the necessary information for reconstructing the topography and morphology of past eruptions from which the pre- and post-eruptive DEMs are derived. It consists of detailed geological mapping of the main volcanic units (cones, tephra air-fall deposits, and lava flows), together with the acquisition of information of geomorphologic (e.g. lava flow thickness), structural, stratigraphic, and, if necessary, bathymetric observations (Figure 1).


This work aims to provide an effective workflow for the pre- and post-eruption topographic and morphometric reconstruction of monogenetic volcanic eruptions and assess related lava flow simulations (Figure 1). As a case study, we test its effectiveness in Montaña de Aguarijo, one of the recent and well-preserved monogenetic volcanoes of El Hierro Island (Canary Islands, Spain). The eruption of Montaña de Aguarijo has the peculiarity of exhibiting a lava flow forming cascades on a coastal cliff and spreading at the cliff base over an old coastal platform reaching into the sea.

2. Geological setting

2.1. Canary Islands

The Canary Islands, which comprise a roughly linear 500 km long east–west aligned chain of seven

CONTACT A. Rodriguez-Gonzalez ✉ franciscojose.perez@ulpgc.es Instituto de Estudios Ambientales y Recursos Naturales (i-UNAT), Universidad de Las Palmas de Gran Canaria (ULPGC), Las Palmas de Gran Canaria, Spain

 Supplemental data for this article can be accessed at <https://doi.org/10.1080/17445647.2021.1972853>.

© 2021 The Author(s). Published by Informa UK Limited, trading as Taylor & Francis Group on behalf of Journal of Maps

This is an Open Access article distributed under the terms of the Creative Commons Attribution License (<http://creativecommons.org/licenses/by/4.0/>), which permits unrestricted use, distribution, and reproduction in any medium, provided the original work is properly cited.

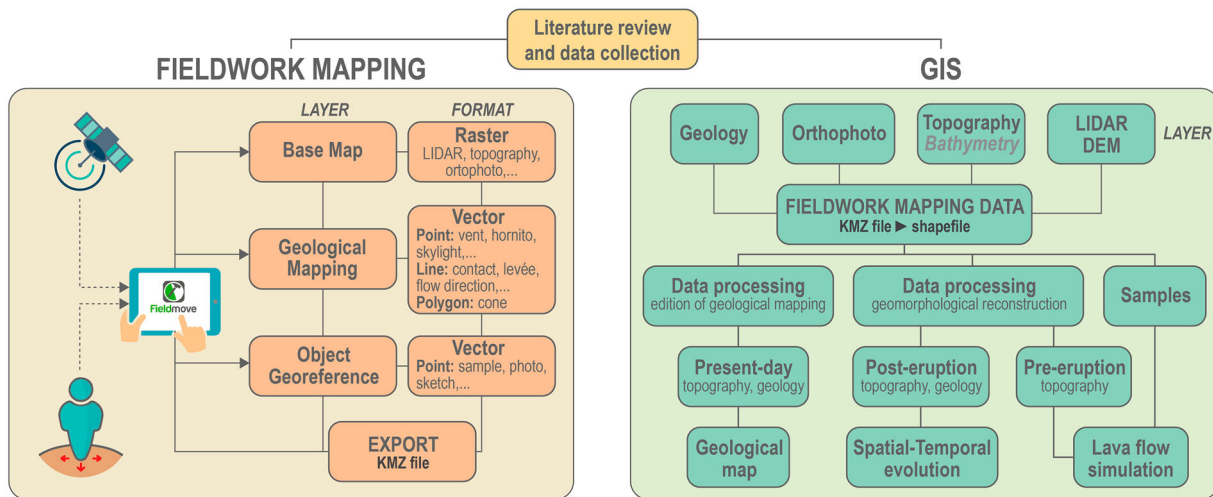


Figure 1. Conceptual flowchart showing the methodology of the fieldwork mapping and GIS study.

main islands and several islets, are located off the north-western African coast, between 29° 25' and 27° 37' N and 18° 10' and 13° 20' W (Figure 2a). This archipelago is preceded by a group of seamounts located further NE and together form the Canary Volcanic Province (CVP), an ~800-km-long and ~400-km-wide volcanic belt. The CVP developed above the Jurassic ocean lithosphere (cold, thick, rigid, and old crust) lying close to the African passive continental margin and on the slow-moving (~2 cm/y) African plate (Silver et al., 1998). Volcanism in the CVP decreases in age from the NE to the SW, from ca. 68 Ma in the

Lars/Essaouira seamount (Geldmacher et al., 2005) to ca. 1.12 Ma in the El Hierro island (Guillou et al., 1996) (see Figure 2a). This age progression is due to the African plate's movement over a mantle plume (e.g. Carracedo, 1999; Geldmacher et al., 2005; Hoernle & Schmincke, 1993; Zaczek et al., 2015).

The Canary archipelago displays, similarly to other intraplate volcanic islands, three main hotspot volcanic stages of evolution: (1) juvenile (shield) stage, (2) volcanic quiescence stage and (3) rejuvenated stage. The westernmost islands (El Hierro and La Palma) are in the juvenile stage, which is

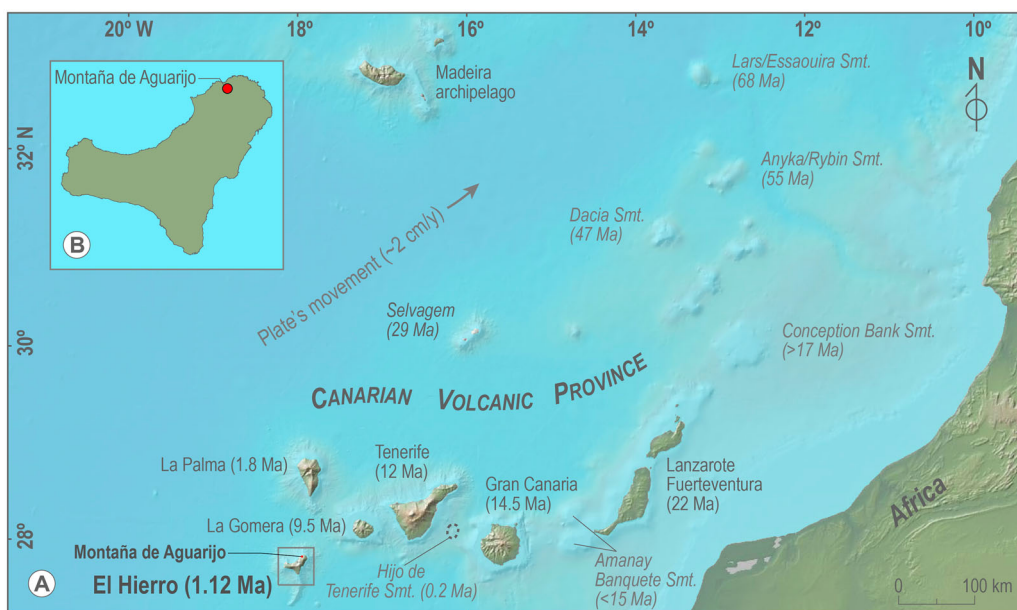


Figure 2. (a) The Canary Volcanic Province, including the main islands and the associated seamounts with ages (Geldmacher et al., 2001; Guillou et al., 2004; Ryan et al., 2009). (b) El Hierro Island ortophotomap and location of Montaña de Aguarijo.

characterised by high eruption rates and fast volcanic growth, whilst the easternmost ones (Fuerteventura and Lanzarote) are in the rejuvenated stage where the erosive processes play a significant role (Carracedo et al., 1998, 2002; Walker, 1990).

2.2. El Hierro

El Hierro, the youngest and westernmost island of the Canarian archipelago, is the emergent area of a 280 km² volcanic shield that rises from ~4000 m deep seafloor to 1502 m above sea level at the centre of the island (Pico Malpaso) (Figure 2b). The most characteristic feature of El Hierro is its tetrahedron shape, with edges formed by three convergent ridges of volcanic cones at 120° and separated by wide embayments.

The subaerial development of the island resulted from the overlapping growth of three main periods: (1) Tiñor Volcano edifice (1.12–0.54 Ma), (2) El Golfo Volcano edifice (545–176 ka) and (3) the recent rift volcanism (<176 ka) (Becerril et al., 2013, 2014, 2016; Carracedo et al., 2001; Guillou et al., 1996). Their rapid and unstable growth turns out to be one of the conditioning factors on the occurrence of the five giant gravitational landslides identified at El Hierro: Tiñor (<880 ka), (2) Las Playas I (545–176 ka) and II (176–145 ka), (3) El Julan (>158 ka), (4) El Golfo (133–21 ka) and (5) Punta del Norte (unknown age) (e.g. Carracedo et al., 1999, 2001; Longpré et al., 2011; Urgeles et al., 1997 and the references therein). A three-armed rift system controls the present-day structure, morphology and recent volcanic eruptions of El Hierro (e.g. Carracedo, 1994, 1996; Carracedo et al., 1999).

Montaña de Aguarijo is a cinder cone located at the north-eastern rift system within 3 km to the capital Valverde and about 5 km to the small airport (El Hierro Airport). Together with Montaña del Tesoro and Montaña Chamuscada represent the principal platform forming eruptions at the NE rift and are thought to be younger than 18 ka BP due to older lavas are arranged to form cliffs (Carracedo et al., 2001). The most particular feature of Montaña de Aguarijo is its 2300 m length lava flow that cascades over the edge of a palaeocliff and spreads over a narrow old shore platform before reaching and plunging into the sea (Figure 3).

3. Materials and methods

3.1. Mapping and palaeogeomorphological reconstruction

Volcanic morphometric modelling included intensive fieldwork to carry out a meticulous geomorphological and topographic reconstruction of the Montaña de

Aguarijo eruption, to obtain the pre- and post-eruption DEMs. Fieldwork identified and analysed the volcanic landforms, i.e. cone, lava flow and levées, besides the underlying palaeorelief (Rodríguez-González et al., 2010, 2012). The geological mapping of these units was performed through a digitising tablet (iPad Pro 11” Wi-Fi + Cellular model + GPS / GNSS receiver) to trace over and vectorise the contact lines and geolocation points (photos, sketches, samples, etc.). For more accurate results, we try the heads-up digitising method with pencil, by which the operator is continuously geolocated, using the FieldMove application. We use high-resolution raster maps as MBtiles files as a reference (background) layer for the digital base map data (e.g. orthophoto, LIDAR, topography) in the FieldMove application. Since the new vector elements are displayed over the reference map image, we can visually check the accuracy as we go along. The vector data structure allows representing the geological data in a single vector object providing the most efficient means to digitise and store the data for a large, complex map. Later, for more flexibility in the map design, we may separate the data into different thematic layers (such as unit contacts, outcropping structures, or individualised eruptions). Finally, the data acquired is exported to a KMZ file and introduced in a GIS environment, which offers valuable capabilities for estimating accurately the morphological parameters and derivatives required, e.g. eruption output volume, slope and aspect of the terrain (Figure 1).

Field-derived data were combined with the available 1:5,000 topographic (Cartográfica de Canarias GRAFCAN, 2006) and 1:1,000 bathymetric (Dirección General de Costas, 2003) digital maps (5 and 1 m contour line equidistance, respectively) to manually modify the present-day contour maps to derive the pre- and post-eruption relief. These modified contour maps were used to obtain the corresponding DEMs in the two different stages: (1) before the eruption modifies the relief (pre-eruption DEM) and (2) just at the end of the eruption, prior to erosive processes (post-eruption DEM). The comparison between these two DEMs and the present-day landform allow us to identify the geomorphological evolution of the study area (Figure 4). In this evolution, three coastlines are recognised (pre- and post-eruption and current coastline). In this scenario, the post-eruption and current coastlines reflect the lava flow fronts that gained land from the sea and later receded due to coastal erosion, respectively. Besides, the distribution and morphology of the bathymetric curves permits the drawing of the advance of the Montaña de Aguarijo lava lobe in a submarine regime.

Obtaining the morphometric parameters of the volcanic cone and lava flow requires different processes depending on if they have a horizontal or vertical

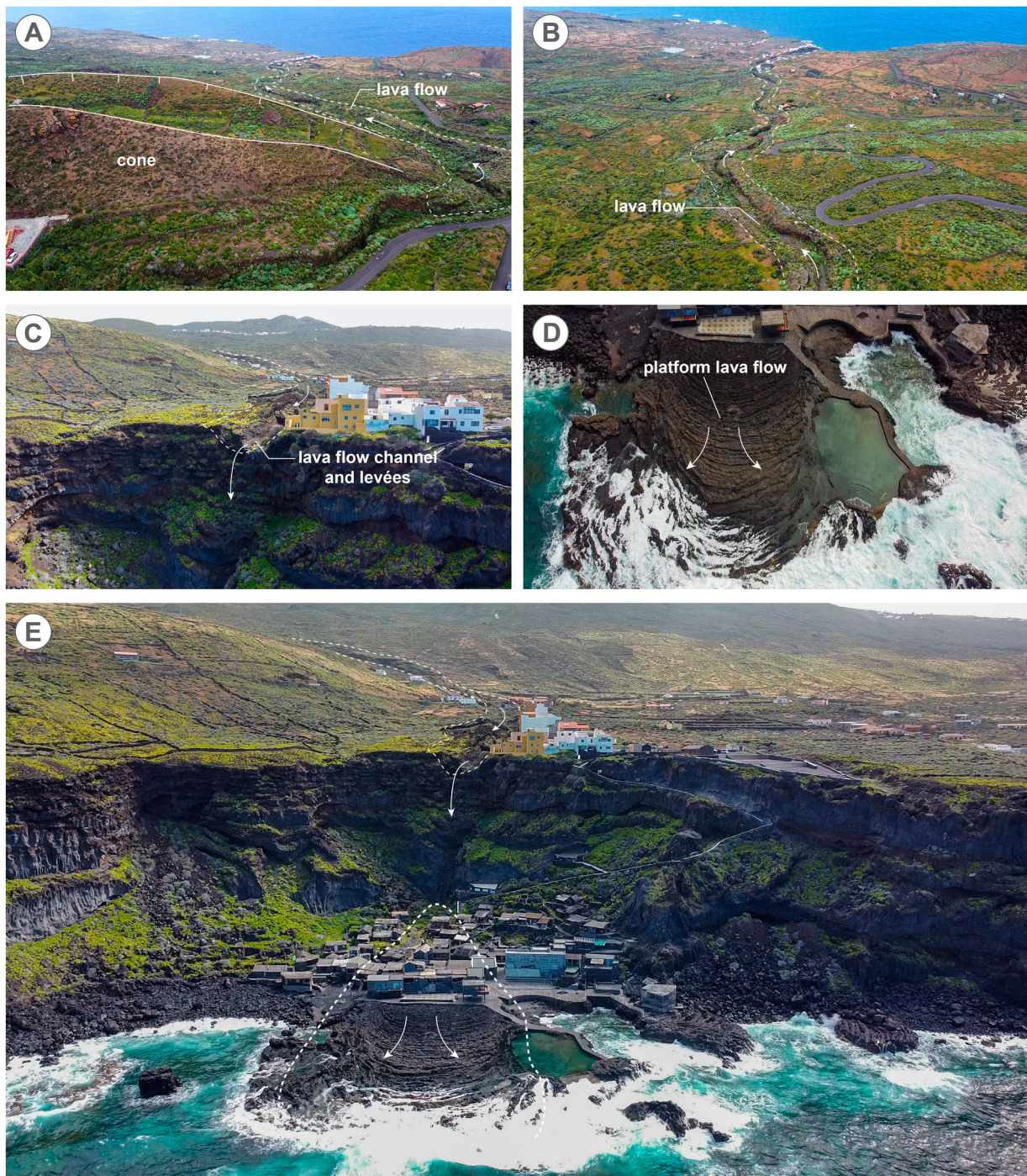


Figure 3. Unmanned Aerial Vehicle (UAV) images of the cone and lava flow of Montaña de Aguarijo eruption. **(a)** Landscape perspective of the cone (bounded crater) and emission of the lava flow at the crater's cone base. **(b)** The landscape of the lava flow in 'Barranco de Las Martas'. **(c)** Cross-section of the lava flow channel in the palaeocliff. **(d)** View zenith of the lava flow forming offshore platform. **(e)** Whole landscape to view lava flow channel in the palaeocliff and lava flow forming offshore platform.

component. Horizontal parameters (i.e. lava flow length or crater rim major and minor axes) were obtained by measuring geotools on GIS software. Vertical parameters (i.e. lava flow thickness and cone height) were derived from comparing the pre- and post-eruption DEMs.

The bulk erupted volume (V_{bulk}) was calculated through GIS methods (cut-and-fill analysis) from the

elevation difference between the pre- and post-eruption DEMs. The obtained value considers the solid and void volumes of the different volcanic units and, therefore, does not represent the absolute volume of the emitted volcanic products. Correction factors assuming a porous volume fraction of 75% for the volcanic cone (Mangan & Cashman, 1996) and 25% for the lava flow (Wolfe et al., 1987) were applied to

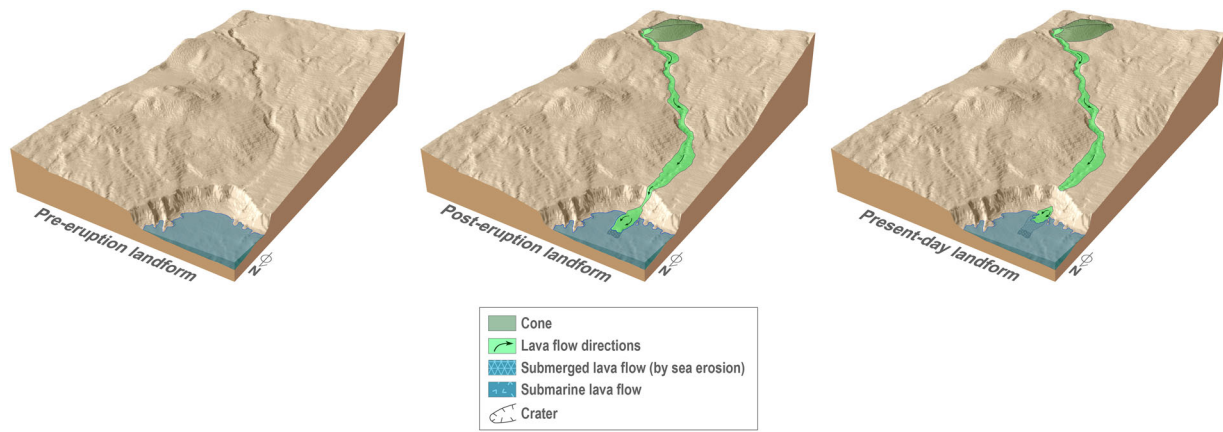


Figure 4. Digital Elevation Models were obtained from the palaeogeomorphological reconstruction of the zone affected by the eruption of Montaña de Aguarijo, showing pre-, post-eruption and present-day geomorphology.

obtain the dense rock equivalent volume (V_{DRE}) (e.g. Rodriguez-Gonzalez et al., 2010, 2011). Comparing the post-eruption and present-day DEMs also helped understand the magnitude and distribution of the erosive processes that have affected Montaña de Aguarijo since its eruption.

The pre-eruption relief of any eruption zone constrains the lava flow velocity, propagation direction, and volcanic cone shape. The pre-eruption DEM of Montaña de Aguarijo and the obtained morphometric parameters were used as input data for the lava flow simulations.

3.2. Q-LavHA simulation models

The Q-LavHA v3.0 freeware plugin (Mossoux et al., 2016), integrated into the QGIS v3.10 software, simulates the probability of inundation by ‘a’ lava flows from one or more eruptive vents spatially distributed on a DEM. Q-LavHA integrates three different models that allow establishing a simulated lava flow path, where the first two are probabilistic and the latter deterministic: (1) Maximum Length (L_{max}), (2) Decreasing Probability (L_{normal}), and (3) FLOWGO (L_{flowgo}).

The L_{normal} alternative has not been applied since it is based on a decreasing cumulative density function (equation 9 of Mossoux et al., 2016), and therefore, requires the average length and standard deviation of previous lava flows with similar behaviour. In this work, we present Montaña de Aguarijo’s lava flow simulation running L_{max} (Felpeto et al., 2001) and L_{flowgo} (Harris & Rowland, 2001) models. In both cases, corrective factors (H_c , minimum thickness and H_p , mean thickness) and the length (L) of the actual lava flow are considered to determine the propagation of the simulated flow and allow it to overcome small topographic obstacles and fill depressions. The number of iterations is also specified, which define the

number of flow lines computed to obtain a good fit between the simulations and the actual lava flow (Mossoux et al., 2016).

The probabilistic maximum length model (L_{max}) considers a maximum length (L') as the distance covered by the lava flow line, estimated by applying a corrective factor to the actual lava flow length. The simulated flow runs from a given emission point over a DEM based on propagation rules, and each iteration stops when the lava flow line reaches the specified maximum length (Mossoux et al., 2016).

The deterministic FLOWGO model (L_{flowgo}) requires the input of multiple physical and rheological parameters that determine the evolution of the simulated lava flow over the topography. The simulation stops when at least one of the following conditions is achieved: (1) the lava velocity is zero, (2) the lava core temperature reaches the solidus, or (3) the yield strength at the base of the channel is greater than the downhill stress (Mossoux et al., 2016). The slope is a critical factor in FLOWGO since it influences the lava flow propagation and cooling speeds, two key parameters that control the final length reached by the lava (Rodriguez-Gonzalez et al., 2019).

To evaluate the accuracy of each simulated lava flow, six fitness indexes (FI ; whose value ranges from 0 to 1) are calculated by Q-LavHA through the same DEM as in the simulation but assigning a value of 1 to the pixels that represent the actual lava flow and a value of 0 to the pixels outside of it. Fitness indexes determine the overlapped ($FI_{true\ positive}$, TP), overestimated ($FI_{false\ positive}$, FP) and underestimated ($FI_{false\ negative}$, FN) areas between the simulated and the actual lava flow. Therefore, the closer the TP value is to 1, the better the correspondence is between both flows. The FP and FN indexes assess whether the divergence between the simulated and actual lava flow is due to an overestimation or underestimation of the area covered by the simulation, helping determine its effective

use in hazard management properly. A weighted composite score ($FI_{composite\ score}$, CS) is also obtained from the TP, FP and FN indexes, whose value reflects the null (0) or maximum (1) coincidence between the simulated and the actual lava flow. Besides, the cumulative flood probability ($FI_{cumulative\ probability}$, CUM) is established for the pixels located inside (FI_{CUMin}) and outside (FI_{CUMout}) the actual lava flow. Therefore, the higher the FI_{CUMin} and the lower the FI_{CUMout} values are, the more accurate the simulation is (Favalli et al., 2009; Mossoux et al., 2016).

4. Modelling and simulation of Montaña de Aguarijo lava flow

4.1. Morphometric modelling

Morphometric parameters and their derivatives of the volcanic cone and lava flow are shown in Tables 1 and 2, respectively. The accuracy of erupted volumes obtained from GIS-based methods is compared with those from classical formulae-derived methods.

4.1.1. Cone

The volcanic cone emerged over a gently N-dipping terrain with a mean slope of $13 \pm 6^\circ$. The cone displays a horseshoe-shaped crater opening to the NE. Crater rim morphology is influenced by the original relief and wind predominance and shows an asymmetric profile defined by the more significant development of its NW flank, where it reaches a maximum height of 500 m. The eccentricity of the cone (0.7) is smaller than the crater (0.9); therefore, the cone shows a more circular shape in plain view. The mean cone slope is $28 \pm 9^\circ$, and its internal structure presents a sequence

Table 1. Morphometric parameters and their derivatives of the volcanic cone from the Montaña de Aguarijo eruption.

Volcanic cone	Symbol	Unit	Value
Crater maximum elevation	h	m	500
Crater rim major axis	a_{cr}	m	302
Crater rim minor axis	b_{cr}	m	129
Crater rim eccentricity	e_{cr}		0.9
Crater major axis azimuth	θ	degrees	47
Crater depth	h_{cr}	m	28
Cone major axis	a_{co}	m	462
Cone minor axis	b_{co}	m	323
Cone eccentricity	e_{co}		0.7
Cone major axis azimuth	θ	degrees	54
Cone height	H	m	65
Cone slope	a		
Median		degrees	28
Mean		degrees	28
Minimum		degrees	0
Maximum		degrees	58
Standard deviation		degrees	9
Basement slope (pre-eruption)	β		
Median		degrees	13
Mean		degrees	13
Minimum		degrees	0
Maximum		degrees	42
Standard deviation		degrees	6
Area	A	m^2	105657
Volume	V	m^3	563096

of coarse-grained beds, ranging from welded scoria and volcanic bombs to lapilli. Considering the morphology of this cone and its pyroclastic materials, it can be categorised as type 2 according to Martin and Németh (2006) classification. Therefore, the cone was generated by strombolian eruptive mechanisms (see Figure 3a).

Cone volumes (V_{DRE}) derived from morphometric modelling and traditional geometric formulae procedures are $563,096\ m^3$ and $4,851,199\ m^3$, respectively, being the latter ~ 8.6 times higher. The volume surplus given by the classical formulae-derived procedures is attributed to the poor intrinsic accuracy of this method, which must not be used in volcanic modelling since it could infer volcanic hazard overestimations (Rodríguez-González et al., 2010).

4.1.2. Lava flow

The lava flow emission occurs at the crater's cone base (see Figure 3a), from where it is channelled along 2000m following the V-shaped ravine named 'Barranco de Las Martas' (Figure 3b) before reaching a palaeocliff border. Once it is reached, it forms cascades that end up coalescing at the cliff base (Figure 3c). Then, lava spreads over a narrow abrasion platform and reaches the sea modifying the coastline (Figure 3d-e). Close to the emission point, morphologies of 'a'ā-type lava with levees are present, whereas pahoehoe arch-forming advancement structures are observed through the small lava platform. Lava flow length is 2268 m, including the submarine section, and its width varies from 17 m at the cliff base to 108 m at the end of the Barranco de Las Martas minor incision zone, with a mean value of 54 ± 23 m. Its thickness varies significantly, from 2 m at the cliff border to 21 m at the Barranco de Las Martas major incision zone, where erratic blocks occur, with a

Table 2. Morphometric parameters and their derivatives of the lava flow from the Montaña de Aguarijo eruption.

Lava flow	Symbol	Unit	Value
Length	L	m	2268
Bottom width	w_b		
Median		m	57
Mean		m	54
Minimum		m	17
Maximum		m	108
Standard deviation		m	23
Height (thickness)	h		
Median		m	5
Mean		m	5
Minimum		m	2
Maximum		m	21
Standard deviation		m	4
Basement slope	β		
Median		degrees	11
Mean		degrees	13
Minimum		degrees	0
Maximum		degrees	31
Standard deviation		degrees	7
Area	A	m^2	115618
Volume	V	m^3	316922

Table 3. Parameters used for the Q-LavHA L_{max} and L_{flowgo} simulations of the lava flow from Montaña de Aguarijo volcano in El Hierro Island.

L_{max} and L_{flowgo} input parameters	Symbol	Unit	Values	Sources
Type of lava			'a'ā	Fieldwork-derived
Emission point (X, Y; WGS84-UTM 28N)		m	210740, 3081349	Fieldwork-derived
DEM resolution		m	10 x 10	
Lava flow length	L	m	2268	GIS-derived
Corrected lava flow length	L'	m	$2268 * 1.24 = 2812$	GIS-derived
Minimum thickness	H_c	m	2	GIS-derived
Mean thickness	H_p	m	5	GIS-derived
Number of iterations			1500	
L_{flowgo} input parameters				
Effusion rate	E_r	$m^3 s^{-1}$	100	
Lava initial viscosity	η	Pa s	2.05	Einstein-Roscoe equation
Initial phenocryst mass fraction	Φ_{phen}	%	0.2	Estimated from thin section
Channel ratio (width/depth)	w/r		10.8	GIS-derived
Thermal parameters				
Eruption temperature	T_{erupt}	°C	1250	
Crust temperature	T_{crust}	°C	600	
Offset	T_{offset}	°C	150	
d constant	d		-0.16	Mossoux et al. (2016)
Velocity constant				
Gravity	g	$m s^{-2}$	9.81	Constant for Earth
Crystal parameters				
Rate of crystallization	df/dT		0.004	
Latent heat of crystallization	L	$J kg^{-1}$	$3.50E+05$	Constant for Earth
Inverse of maximum crystal concentration	R		1.51	
Viscosity and elasticity				
a constant	a	K^{-1}	0.04	Dragoni (1989)
b constant	b	Pa	0.01	Dragoni (1989)
c constant	c	K^{-1}	0.08	Dragoni (1989)
Lava density and vesicularity				
Bulk density	ρ_{bulk}	$kg m^{-3}$	2802	Bottinga and Weill equation
DRE density	ρ_{DRE}	$kg m^{-3}$	2859	DRE density = bulk density/ 1-vesicularity
Vesicularity	Φ_b	%	0.02	Estimated from thin section
Radiation parameters				
Stefan-Boltzmann constant	σ	$W m^{-2} K^{-4}$	$5.67E-08$	Constant for Earth
Emissivity of basalt	ϵ		0.95	Constant for Earth
Convection parameters				
Wind speed	U	$m s^{-1}$	5	
Ch	C_h		0.0036	Constant for Earth
Air temperature	T_{air}	°C	25	
Air density	ρ_{air}	$kg m^{-3}$	0.4412	Constant for Earth
Air specific heat capacity	$c\rho_{air}$	$J kg^{-1} K^{-1}$	1099	Constant for Earth
Conduction parameters				
Thickness of lava crust	H_b	%	10	
Temperature at base of lava crust	T_{base}	°C	600	
Lava thermal conductivity	k_{lava}	$W m^{-1} K^{-1}$	2.05	

mean value of 5 ± 4 m. Fluvial erosion only affects the N flank since the lava channel itself and the slopes through which it flows facilitate water transport. However, coastal erosion significantly impacts the lava advancement front, causing it to recede several metres, leaving isolated rocks as evidence.

Lava flow volumes (V_{DRE}) obtained from morphometric modelling and traditional geometric formulae procedures are $316,922 m^3$ and $459,270 m^3$, respectively, the latter ~ 1.4 times higher. Overestimation is also related to the poor intrinsic accuracy of formulae-derived calculations. Thus, GIS-based methods provide more accurate volume estimations either for the volcanic cone or the lava flow.

4.2. Lava flow simulations

Calculated and constant standard parameters used as input data for lava flow simulations are presented in Table 3. Q-LavHA does not consider lava flow-

seawater interaction (which slows down the lava flow velocity) and the bathymetric information of the DEM, a handicap for correctly simulating lava flows that extend beyond the coastline. However, assuming that the flooding risk of the Montaña de Aguarijo lava flow offshore is null, the DEM used for the simulations in this work is cut and only considers the subaerial path of the flow.

4.2.1. Probabilistic maximum length constraint (L_{max})

The probabilistic constraint L_{max} depends exclusively on the pre-eruption topography, the lava flow's maximum length, and its minimum and average thicknesses (Table 3). The simulation derived from this approach (see Main Map) is similar to the actual lava flow and shows that the major inundation probability is focused within the central area of the channel. The main zones where the morphology of the simulated lava flow overestimates the real one are

also those with a lower inundation probability (see Main Map): (1) near the emission centre, where the simulation runs through a narrow channel semi-parallel to the main flow, (2) at the simulation midpoint, where the NE and SW areas adjacent to the actual lava flow are inundated, and (3) close to the paleo-cliff termination zone, where the simulation floods the western sectors of the actual lava flow. Contrarily, the underestimated areas are scarce, reduced and mainly located ~500 m far from the emission centre (SW sector adjacent to the main channel) and in the lava flow termination (E sector adjacent to the main channel).

According to the calculated *FIs*, the overlap (*TP*), overestimation (*FP*) and underestimation (*FN*) percentages of the simulated lava flow are 43.6%, 48.5% and 7.9%, respectively. The composite score (*CS*) reveals a 26.5% match between the simulated and real lava flow, while the cumulative flood probabilities (*CUM*) for the pixels located inside (FI_{CUMin}) and outside (FI_{CUMout}) the actual flow are 94.1% and 5.9%, respectively. These percentages reveal that the pixels with the highest flood probability match with the actual lava flow and thus that the simulation is correctly adjusted to reality since the input parameters are close to the actual eruption features (Favalli et al., 2009; Mossoux et al., 2016).

4.2.2. Deterministic FLOWGO constraint (L_{flowgo})

The deterministic model L_{flowgo} considers a set of physical and rheological parameters that determine the lava flow's speed, trajectory, and evolution, in addition to the morphometric parameters already considered in the L_{max} approach. The simulation obtained by this method (see Main Map) shows significant similarities with L_{max} , being the highest flood probability areas located in the central part of the channel flow.

The *FIs* show a degree of overlap (*TP*) between the simulated and real lava flows of 42.2%, with 53.7% of pixels overestimated (*FP*) and 4.1% underestimated (*FN*). According to the *CS*, the coincidence between the simulated and real lava flow is 26.5%, with cumulative flood probabilities of 93.6% for the overlapping pixels (FI_{CUMin}) and 6.4% for the non-overlapping pixels (FI_{CUMout}). Thus, the L_{flowgo} model, which considers a greater number of parameters than L_{max} , also offers accurate results of the lava flow simulation.

The physical and rheological parameters considered in L_{flowgo} are close to the actual characteristics of the Montaña de Aguarijo lava flow. Therefore, these values could serve as a precedent for the simulation of other lava flows in El Hierro or other intraplate volcanic islands with similar eruptive dynamics since they can be considered the parameters that will control the development of future effusive eruptions.

5. Conclusions

The compilation of maps of Montaña de Aguarijo's eruption (El Hierro, Canary Islands) illustrates the accuracy of the proposed methodology. Field mapping and generation of 2D and 3D reconstructions allow calculating Montaña de Aguarijo morphometric parameters used as input data to simulate the lava flow inundation probability. The comparison between the resulting probabilistic and deterministic maps shows a high level of correspondence, demonstrating the methodology's usefulness in assessing and forecasting the areas potentially affected by future eruptions on the island.

Software

Georeferencing and digitisation of the eruption were performed initially using GeoPads equipped with the Digital Field Mapping System FieldMove to trace over and vectorise the contact lines. Data processing and development necessary to elaborate the map were performed using TNTGIS 2019 and QGIS 3.10 and 3.16 with the plugin Q-LavHA. The 3D images on the map were produced using the TNTGIS 2019. The GeoMap application was used for bathymetric maps and Microsoft Excel 2016 to calculate morphometric and simulation lava flow parameters. The topographic profiles were produced using the profile tool QGIS 3.16. The final design was carried out using Adobe Illustrator 2020.

Data availability statement

The authors confirm that the data supporting the findings of this study are available within the article.

Geolocation information

name = El Lajial, El Hierro Island, Canary Islands, Spain; geonames = <https://www.geonames.org/12225645/montana-de-aguarijo.html>; westBoundLongitude = -17,949; eastBoundLongitude = -17,936; southBoundLatitude = 27,822; northBoundLatitude = 27,843

Acknowledgements

Financial support was provided by Project LAJIAL (ref. PGC2018-101027-B-I00, MCIU/AEI/FEDER, EU). This study was carried out in the framework of the Research Consolidated Groups GEOVOL (Canary Islands Government, ULPGC) and GEOPAM (Generalitat de Catalunya, 2017 SGR 1494). We thank the collaboration of S. Díaz Rodríguez with the UAV images. We are grateful to the editor M. J. Smith for the effective handling of the manuscript and Makram Murad-al-shaikh, J. Galve and G. Groppelli for providing insightful comments on a preliminary version of this work.

Disclosure statement

The authors reported no potential conflict of interest.

Funding

The research carried out to develop this map, including fieldwork, geomorphology, petrology and geochemistry, was funded by Project LAJIAL (ref. PGC2018-101027-B-I00, MCIU/AEI/FEDER, EU); Ministry of Science, Innovation and Universities (<https://doi.org/10.13039/100014440>).

ORCID

C. Prieto-Torrell  <http://orcid.org/0000-0002-8707-6803>
 A. Rodriguez-Gonzalez  <http://orcid.org/0000-0003-0688-0531>
 M. Aulinas  <http://orcid.org/0000-0003-3795-3537>
 J. L. Fernandez-Turiel  <http://orcid.org/0000-0002-4383-799X>
 M.C. Cabrera  <http://orcid.org/0000-0002-4556-4665>
 C. Criado  <http://orcid.org/0000-0002-5062-0561>
 F. J. Perez-Torrado  <http://orcid.org/0000-0002-4644-0875>

References

- Becerril, L., Bartolini, S., Sobrado, R., Martí, J., Morales, J. M., & Galindo, I. (2014). Long-term volcanic hazard assessment on El Hierro (Canary Islands). *Natural Hazards and Earth System Sciences*, 14(7), 1853–1870. <https://doi.org/10.5194/nhess-14-1853-2014>
- Becerril, L., Cappello, A., Galindo, I., Neri, M., & Del Negro, C. (2013). Spatial probability distribution of future volcanic eruptions at El Hierro Island (Canary Islands, Spain). *Journal of Volcanology and Geothermal Research*, 257, 21–30. <https://doi.org/10.1016/j.jvolgeores.2013.03.005>
- Becerril, L., Galve, J. P., Morales, J. M., Romero, C., Sánchez, N., Martí, J., & Galindo, I. (2016). Volcano-structure of El Hierro (Canary Islands). *Journal of Maps*, 12(sup1), 43–52. <https://doi.org/10.1080/17445647.2016.1157767>
- Cappello, A., Ganci, G., Calvari, S., Pérez, N. M., Hernández, P. A., Silva, S. V., Cabral, J., & Del Negro, C. (2016). Lava flow hazard modeling during the 2014–2015 Fogo eruption, Cape Verde. *Journal of Geophysical Research: Solid Earth*, 121(4), 2290–2303. <https://doi.org/10.1002/2015JB012666>
- Carracedo, J. C. (1994). The Canary Islands: An example of structural control on the growth of large oceanic-island volcanoes. *Journal of Volcanology and Geothermal Research*, 60(3–4), 225–241. [https://doi.org/10.1016/0377-0273\(94\)90053-1](https://doi.org/10.1016/0377-0273(94)90053-1)
- Carracedo, J. C. (1996). A simple model for the genesis of large gravitational landslide hazards in the Canary Islands. *Geological Society, London, Special Publications*, 110(1), 125–135. <https://doi.org/10.1144/GSL.SP.1996.110.01.10>
- Carracedo, J. C. (1999). Growth, structure, instability and collapse of Canarian volcanoes and comparisons with Hawaiian volcanoes. *Journal of Volcanology and Geothermal Research*, 94(1–4), 1–19. [https://doi.org/10.1016/S0377-0273\(99\)00095-5](https://doi.org/10.1016/S0377-0273(99)00095-5)
- Carracedo, J. C., Day, S., Guillou, H., Rodriguez-Badiola, E., Canas, J. A., & Perez-Torrado, F. J. (1998). Hotspot volcanism close to a passive continental margin: The Canary Islands. *Geological Magazine*, 135(5), 591–604. <https://doi.org/10.1017/S0016756898001447>
- Carracedo, J. C., Day, S. J., Guillou, H., & Perez-Torrado, F. J. (1999). Giant Quaternary landslides in the evolution of La Palma and El Hierro, Canary Islands. *Journal of Volcanology and Geothermal Research*, 94(1–4), 169–190. [https://doi.org/10.1016/S0377-0273\(99\)00102-X](https://doi.org/10.1016/S0377-0273(99)00102-X)
- Carracedo, J. C., Perez-Torrado, F. J., Ancochea, E., Meco, J., Hernán, F., Cubas, C. R., Casillas, R., Rodriguez-Badiola, E., & Ahijado, A. (2002). Cenozoic volcanism II: The Canary Islands. In W. Gibbons, & T. Moreno (Eds.), *The Geology of Spain* (pp. 439–472). Geological Society of London. <https://doi.org/10.1144/GOSPP.18>
- Carracedo, J. C., Rodriguez-Badiola, E., Guillou, H., de la Nuez, J., & Perez-Torrado, F. J. (2001). Geology and volcanology of La Palma and El Hierro, Western Canaries. *Estudios Geológicos*, 57(5–6), 175–273. <https://doi.org/10.3989/egol.01575-6134>
- Cartográfica de Canarias GRAFCAN. (2006). Base Topográfica a escala 1:5.000 de El Hierro (2004–2006). Canary Islands Government, Spain.
- Cordonnier, B., Lev, E., & Garel, F. (2015). Benchmarking lava-flow models. *Geological Society, London, Special Publications*, 426(1), 425–445. <https://doi.org/10.1144/SP426.7>
- Damiani, M. L., Groppelli, G., Norini, G., Bertino, E., Gigliuto, A., & Nucita, A. (2006). A lava flow simulation model for the development of volcanic hazard maps for Mount Etna (Italy). *Computers & Geosciences*, 32(4), 512–526. <https://doi.org/10.1016/j.cageo.2005.08.011>
- de' Michieli Vitturi, M., & Tarquini, S. (2018). Mrlavaloba: A new probabilistic model for the simulation of lava flows as a settling process. *Journal of Volcanology and Geothermal Research*, 349, 323–334. <https://doi.org/10.1016/j.jvolgeores.2017.11.016>
- Dietterich, H. R., Lev, E., Chen, J., Richardson, J. A., & Cashman, K. V. (2017). Benchmarking computational fluid dynamics models of lava flow simulation for hazard assessment, forecasting, and risk management. *Journal of Applied Volcanology*, 6(1), 9. <https://doi.org/10.1186/s13617-017-0061-x>
- Dirección General de Costas. (2003). Estudio ecocartográfico del litoral de las islas de El Hierro y La Gomera (Tenerife). Ministry of the Environment.
- Dragonì, M. (1989). A dynamical model of lava flows cooling by radiation. *Bulletin of Volcanology*, 51(2), 88–95. <https://doi.org/10.1007/BF01081978>
- Favalli, M., Karátson, D., Mazzarini, F., Pareschi, M. T., & Boschi, E. (2009). Morphometry of scoria cones located on a volcano flank: A case study from Mt. Etna (Italy), based on high-resolution LiDAR data. *Journal of Volcanology and Geothermal Research*, 186(3–4), 320–330. <https://doi.org/10.1016/j.jvolgeores.2009.07.011>
- Felpeto, A., Araña, V., Ortiz, R., Astiz, M., & García, A. (2001). Assessment and modelling of lava flow hazard on Lanzarote (Canary Islands). *Natural Hazards*, 23(2/3), 247–257. <https://doi.org/10.1023/A:101112330766>
- Geldmacher, J., Hoernle, K., Bogaard, P. v. d., Duggen, S., & Werner, R. (2005). New 40Ar/39Ar age and geochemical data from seamounts in the Canary and Madeira volcanic provinces: Support for the mantle plume hypothesis. *Earth and Planetary Science Letters*, 237(1–2), 85–101. <https://doi.org/10.1016/j.epsl.2005.04.037>
- Geldmacher, J., Hoernle, K., van den Bogaard, P., Zankl, G., & Garbe-Schönberg, D. (2001). Earlier history of the ≥70-Ma-old Canary hotspot based on the temporal and geochemical evolution of the Selvagen Archipelago and

- neighboring seamounts in the eastern North Atlantic. *Journal of Volcanology and Geothermal Research*, 111(1–4), 55–87. [https://doi.org/10.1016/S0377-0273\(01\)00220-7](https://doi.org/10.1016/S0377-0273(01)00220-7)
- Guillou, H., Carracedo, J. C., Perez-Torrado, F. J., & Rodriguez-Badiola, E. (1996). K-Ar ages and magnetic stratigraphy of a hotspot-induced, fast grown oceanic island: El Hierro, Canary Islands. *Journal of Volcanology and Geothermal Research*, 73(1–2), 141–155. [https://doi.org/10.1016/0377-0273\(96\)00021-2](https://doi.org/10.1016/0377-0273(96)00021-2)
- Guillou, H., Perez-Torrado, F. J., Hansen-Machin, A. R., Carracedo, J. C., & Gimeno, D. (2004). The Plio-Quaternary volcanic evolution of Gran Canaria based on new K–Ar ages and magnetostratigraphy. *Journal of Volcanology and Geothermal Research*, 135(3), 221–246. <https://doi.org/10.1016/j.jvolgeores.2004.03.003>
- Harris, A., & Rowland, S. K. (2001). FLOWGO: A kinematic thermo-rheological model for lava flowing in a channel. *Bulletin of Volcanology*, 63(1), 20–44. <https://doi.org/10.1007/s004450000120>
- Hoernle, K., & Schmincke, H.-U. (1993). The role of partial melting in the 15-Ma geochemical evolution of Gran Canaria: A blob model for the Canary Hotspot. *Journal of Petrology*, 34(3), 599–626. <https://doi.org/10.1093/petrology/34.3.599>
- Longpré, M.-A., Chadwick, J. P., Wijbrans, J., & Iping, R. (2011). Age of the El Golfo debris avalanche, El Hierro (Canary Islands): New constraints from laser and furnace $^{40}\text{Ar}/^{39}\text{Ar}$ dating. *Journal of Volcanology and Geothermal Research*, 203(1), 76–80. <https://doi.org/10.1016/j.jvolgeores.2011.04.002>
- Mangan, M. T., & Cashman, K. V. (1996). The structure of basaltic scoria and reticulite and inferences for vesiculation, foam formation, and fragmentation in lava fountains. *Journal of Volcanology and Geothermal Research*, 73(1–2), 1–18. [https://doi.org/10.1016/0377-0273\(96\)00018-2](https://doi.org/10.1016/0377-0273(96)00018-2)
- Martin, U., & Németh, K. (2006). How Strombolian is a “Strombolian” scoria cone? Some irregularities in scoria cone architecture from the Transmexican Volcanic Belt, near Volcán Ceboruco, (Mexico) and Al Haruj (Libya). *Journal of Volcanology and Geothermal Research*, 155(1–2), 104–118. <https://doi.org/10.1016/j.jvolgeores.2006.02.012>
- Mossoux, S., Saey, M., Bartolini, S., Poppe, S., Canters, F., & Kervyn, M. (2016). Q-LAVHA: A flexible GIS plugin to simulate lava flows. *Computers & Geosciences*, 97, 98–109. <https://doi.org/10.1016/j.cageo.2016.09.003>
- Nieto-Torres, A., Guimarães, L. F., Bonadonna, C., & Frischknecht, C. (2021). A new inclusive volcanic risk ranking, part 1: Methodology. *Frontiers in Earth Science*, 9, 672. <https://doi.org/10.3389/feart.2021.697451>
- Richter, N., Favalli, M., de Zeeuw-van Dalzen, E., Fornaciai, A., da Silva Fernandes, R. M., Pérez, N. M., Levy, J., Victória, S. S., & Walter, T. R. (2016). Lava flow hazard at Fogo Volcano, Cabo Verde, before and after the 2014–2015 eruption. *Natural Hazards and Earth System Sciences*, 16(8), 1925–1951. <https://doi.org/10.5194/nhess-16-1925-2016>
- Rodriguez-Gonzalez, A., Aulinas, M., Mossoux, S., Perez-Torrado, F. J., Fernandez-Turiel, J. L., Cabrera, M., & Prieto-Torrell, C. (2021). Comparison of real and simulated lava flows in the Holocene volcanism of Gran Canaria (Canary Islands, Spain) with Q-LavHA: Contribution to volcanic hazard management. *Natural Hazards*, 107, 1785–1819. <https://doi.org/10.1007/s11069-021-04660-6>
- Rodriguez-Gonzalez, A., Aulinas, M., Mossoux, S., Perez-Torrado, F. J., Fernandez-Turiel, J. L., & Moreno-Medina, C. (2019). Modelización del flujo de lava del volcán Pico de Bandama (Gran Canaria, Islas Canarias). *Geogaceta*, 65, 19–22. <http://hdl.handle.net/10261/190067>
- Rodriguez-Gonzalez, A., Fernandez-Turiel, J. L., Perez-Torrado, F. J., Aulinas, M., Carracedo, J. C., Gimeno, D., Guillou, H., & Paris, R. (2011). GIS methods applied to the degradation of monogenetic volcanic fields: A case study of the Holocene volcanism of Gran Canaria (Canary Islands, Spain). *Geomorphology*, 134(3–4), 249–259. <https://doi.org/10.1016/j.geomorph.2011.06.033>
- Rodriguez-Gonzalez, A., Fernandez-Turiel, J. L., Perez-Torrado, F. J., Gimeno, D., & Aulinas, M. (2010). Geomorphological reconstruction and morphometric modelling applied to past volcanism. *International Journal of Earth Sciences*, 99(3), 645–660. <https://doi.org/10.1007/s00531-008-0413-1>
- Rodriguez-Gonzalez, A., Fernandez-Turiel, J. L., Perez-Torrado, F. J., Paris, R., Gimeno, D., Carracedo, J. C., & Aulinas, M. (2012). Factors controlling the morphology of monogenetic basaltic volcanoes: The Holocene volcanism of Gran Canaria (Canary Islands, Spain). *Geomorphology*, 136(1), 31–44. <https://doi.org/10.1016/j.geomorph.2011.08.023>
- Ryan, W. B. F., Carbotte, S. M., Coplan, J. O., O’Hara, S., Melkonian, A., Arko, R., Weissel, R. A., Ferrini, V., Goodwillie, A., Nitsche, F., Bonczkowski, J., & Zemsky, R. (2009). Global multi-resolution topography synthesis. *Geochemistry, Geophysics, Geosystems*, 10(3), Q03014. <https://doi.org/10.1029/2008GC002332>
- Sieron, K., Ferrés, D., Siebe, C., Constantinescu, R., Capra, L., Connor, C., Connor, L., Groppelli, G., & González Zuccolotto, K. (2019). Ceboruco hazard map: Part II—modeling volcanic phenomena and construction of the general hazard map. *Natural Hazards*, 96(2), 893–933. <https://doi.org/10.1007/s11069-019-03577-5>
- Silver, P. G., Russo, R. M., & Lithgow-Bertelloni, C. (1998). Coupling of south American and African plate motion and plate deformation. *Science*, 279(60), 60–63. <https://doi.org/10.1126/science.279.5347.60>
- Tarquini, S., de’ Michieli Vitturi, M., Jensen, E. H., Pedersen, G. B. M., Barsotti, S., Coppola, D., & Pfeffer, M. A. (2019). Modeling lava flow propagation over a flat landscape by using MrLavaLoba: The case of the 2014–2015 eruption at Holuhraun, Iceland. *Annals of Geophysics*, 62(2), 1–18. <https://doi.org/10.4401/ag-7812>
- Urgeles, R., Canals, M., Baraza, J., Alonso, B., & Masson, D. (1997). The most recent megalandslides of the Canary Islands: El Golfo debris avalanche and Canary debris flow, west El Hierro Island. *Journal of Geophysical Research*, 102(B9), 20305–20323. <https://doi.org/10.1029/97JB00649>
- Walker, G. P. L. (1990). Geology and Volcanology of the Hawaiian Islands. *Pacific Science*, 44(4), 315–347.
- Wolfe, E. W., Garcia, M. O., Jackson, D. B., Koyanagi, R. Y., Neal, C. A., & Okamura, A. T. (1987). The Puu Oo eruption of Kilauea Volcano, episodes 1–20, January 3, 1983, to June 8, 1984. *U.S. Geological Survey Professional Paper 1350, 1*, 471–508.
- Zacsek, K., Troll, V. R., Cachao, M., Ferreira, J., Deegan, F. M., Carracedo, J. C., Soler, V., Meade, F. C., & Burchardt, S. (2015). Nannofossils in 2011 El Hierro eruptive products reinstate plume model for Canary Islands. *Scientific Reports*, 5(1), 7945. <https://doi.org/10.1038/srep07945>